Femtosecond dynamics of photoinduced molecular detachment from halogenated alkanes. II. Asynchronous concerted elimination of I_2 from CH_2I_2

Qingguo Zhang,[a] Una Marvet, and Marcos Dantus[b]
Department of Chemistry and Center for Fundamental Materials Research, Michigan State University, East Lansing, Michigan 48824-1322

(Received 30 January 1998; accepted 12 June 1998)

The photoinduced molecular detachment dynamics of CH_2I_2 have been investigated with femtosecond time resolution. Upon multiphoton excitation of CH_2I_2 with 312 nm femtosecond pulses, weak fluorescence in the 260–290 nm region was observed in addition to the I_2 fluorescence in the 290–345 nm region studied in the previous paper. The weak fluorescence has also been interpreted as due to emission from I_2, where I_2 was produced from the photodissociation process $CH_2I_2 \rightarrow CH_2 + I_2^*$. In order to investigate the detailed dynamics of this reaction, femtosecond time-resolved data have been obtained by selective detection of the I_2 fluorescence at 272 and 285 nm. From these transients, it has been found that the dissociation process takes place within the temporal width (50 fs) of the laser pulse and that the I_2 photofragments exhibit coherent vibrational motion. The 272 nm transients also exhibit clear, fast decaying rotational anisotropy, quantitative analysis of which reveals a distribution of rather high rotational levels of I_2. This permits us to conclude that the I_2 detachment is an asynchronous concerted process; while breaking of the two C—I bonds and formation of the I—I bond happen in a single kinetic step, one of the C—I bonds breaks faster than the other. In addition, energy partitioning between the CH_2 and I_2 photofragments has also been explored based on the experimental observations. Since this study involves a multiphoton transition, a theoretical formulation for the time dependent rotational anisotropy is presented for the general case of multiphoton pump and multiphoton probe transitions. © *1998 American Institute of Physics.* [S0021-9606(98)02435-0]

I. INTRODUCTION

This paper is the second in a series of articles designed to unravel the photodissociation dynamics of dihaloalkanes. In the previous paper[1] (referred to as paper I henceforth), we have analyzed the transition state dynamics of the molecular detachment process leading to halogens in the D' state. Here we will investigate in detail the mechanism and dynamics of the reaction leading to the higher excited states of I_2, which fluoresce in the 260–290 nm spectral region.

The past two decades have witnessed growing interest in the spectroscopy and photodissociation dynamics of CH_2I_2,[1–25] the majority of which are concerned with dissociation of a single C—I bond from low-lying excited electronic potential energy surfaces.[2–13] When excited with high energy photon(s), CH_2I_2 molecules are known[1,17–25] to undergo molecular detachment, i.e., $CH_2I_2 \rightarrow CH_2 + I_2^*$. This produces a highly electronically excited I_2 molecule, which fluoresces in a wide range of the spectrum. When CH_2I_2 was irradiated with a Kr resonance lamp (emitting at 116.5 and 123.6 nm), Okabe *et al.*[21] observed weak fluorescence bands in the 180–240 (I_2 $H \rightarrow X$), 250–300 (I_2 $F \rightarrow X$) and 450–500 nm regions in addition to the dominant I_2 $D' \rightarrow A'$ fluorescence in the 290–345 nm region. The quantum yield for the strongest I_2 $D' \rightarrow A'$ fluorescence was measured to be less than 1%.[21,24] The 250–300 and the 450–500 nm fluorescence systems were found to be at least another order of magnitude weaker than the 300–350 fluorescence, while the 180–240 nm fluorescence is the weakest of all.[21]

I_2 fluorescence resulting from two-photon excitation of CH_2I_2 at 248 nm as obtained by Fotakis *et al.*[20] revealed a completely different fluorescence intensity pattern, with the I_2 $F \rightarrow X$ fluorescence being the strongest. The two-photon absorption was thought to cause a two-electron excitation of CH_2I_2.[20] Aside from the molecular detachment pathway, Fotakis *et al.*[20] also observed extensive fragmentation of CH_2I_2, leading to the formation of CH and C fragments.

Although the short time dynamics of the photodissociation channel $CH_2I_2 \rightarrow CH_2I + I$ has been studied extensively using various spectroscopic and time-resolved techniques,[7–12] time-resolved study of the molecular detachment pathway $CH_2I_2 \rightarrow CH_2 + I_2$ had not been performed until our first observation of the coherent vibration in the nascent I_2 fragment.[17] Since then, a series of concerted efforts have been made to unravel the detailed dynamics of this molecular detachment pathway.[1,17–19,25] In paper I, we have presented observations and analysis of the photoinduced molecular detachment dynamics of gem-dihaloalkanes. It was found that multiphoton excitation of all the molecules studied at 312 nm gives rise to fluorescence bands assignable to the $D' \rightarrow A'$ transition of the appropriate molecular halogen. Analysis of the transients indicates that the dissociation processes take place on the order of the temporal duration of the laser pulse

[a]Current address: George R. Harrison Spectroscopy Laboratory, Massachusetts Institute of Technology, Cambridge, MA 02139.
[b]Author to whom correspondence should be addressed.

(~50 fs). For methylene iodide, CH_2I_2, vibrational coherence of the I_2 fragments was observed in the time-resolved transients. These observations clearly suggest that the dissociation reaction is a concerted process, i.e., it happens in a single kinetic step. However, this in no way implies that the breaking of two C—I bonds and the formation of an I—I bond in the photodissociation reaction $CH_2I_2 \rightarrow CH_2 + I_2$ happen simultaneously. In fact, the timing of these elementary events will be one of the major mechanistic questions to be addressed in this study.

As mentioned in paper I, we were unable to extract rotational anisotropy information from the time-resolved transients because of the dominant time zero feature presented in the photodissociation channels yielding halogen molecules in the D' state. In this paper, we report the femtosecond time-resolved investigation of a different photodissociation channel of CH_2I_2. The absence of the time zero feature in some transients allows fast decaying rotational anisotropy to be observed unequivocally. Although the experimental data were obtained using a multiphoton pump transition, the existing theoretical treatment of time dependent rotational anisotropy is applicable to schemes involving only one-photon pump and one-photon probe. Therefore, quantitative analysis of the rotational anisotropy obtained in this study requires generalizing the existing formulation. We have developed a theoretical treatment of the rotational anisotropy that is applicable to schemes involving multiphoton pump and multiphoton probe transitions. This new formulation was subsequently used to extract the rotational distribution of the photofragments from the experimentally determined rotational anisotropy. The rotational distribution then allows the detailed photodissociation mechanism to be inferred.

This paper will be organized as follows. In Sec. II a derivation of time dependent rotational anisotropy will be presented for the case of multiphoton pump and multiphoton probe. This is followed by a description of the experimental data in Sec. III. In Sec. IV, the implications of the results will be explored, with particular emphasis on the photodissociation mechanism.

II. THEORY

A. Rotational anisotropy

Time-dependent rotational anisotropy has been discussed by many authors.[19,26–32] However, all these formulations are only applicable to the situation of one-photon pump and one-photon probe. Since the pump-probe scheme employed in this study involves a multiphoton transition, it is necessary to develop a formulation that is applicable to experiments involving multiphoton pump and multiphoton probe transitions. Thus, the following treatment will assume that a delta function-like pump pulse at time zero excites an *m*-photon transition and a delta function-like probe pulse at a delayed time *t* excites an *n*-photon transition. Note that the following treatment is equally applicable to bound-bound, bound-free and free-bound transitions.

Let $\hat{\epsilon}_1$ and $\hat{\epsilon}_2$ be the unit electric polarization vectors for the pump and probe pulses, respectively (see Fig. 1). Let $\hat{\mu}_1(0)$ and $\hat{\mu}_2(t)$ be unit vectors along the directions of the pump and probe transition dipoles, respectively. The 0 and *t* in the parentheses of $\hat{\mu}_1(0)$ and $\hat{\mu}_2(t)$ signify the respective instances when the pump and probe pulses are switched on. Each of the *m* pump dipoles, $\hat{\mu}_1(0)$, is assumed to be parallel to each other, as is each of the *n* probe dipoles, $\hat{\mu}_2(t)$. These are valid assumptions because molecules usually rotate to a negligible degree within the duration of a femtosecond pulse; therefore, the orientation of transition dipoles can be considered essentially stationary within this period. Thus, multiphoton transitions with femtosecond pulses are much less likely if some of the transition dipoles are perpendicular to each other than if they are all parallel.

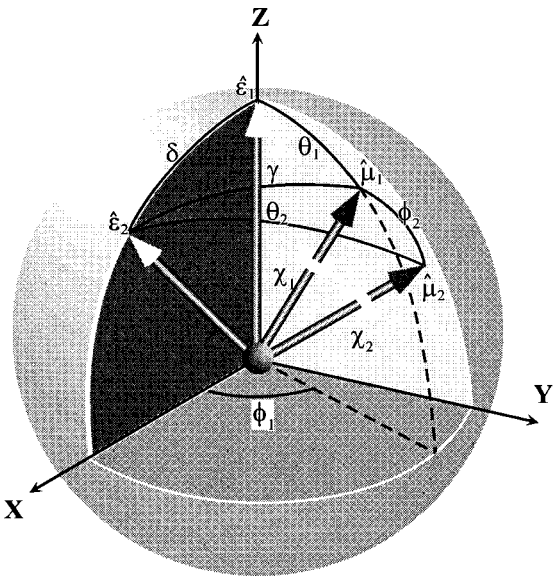

FIG. 1. Definitions of the polarization and transition dipole vectors and the angles among them. The space-fixed vectors $\hat{\epsilon}_1$ and $\hat{\epsilon}_2$ denote, respectively, the unit vectors along the pump and probe electric polarization directions. The molecule-fixed vectors $\hat{\mu}_1$ and $\hat{\mu}_2$ are the dipoles of the pump and the probe transitions. Since the pump pulse defines the time zero, $\hat{\mu}_1$ is meaningful only at time zero, i.e., $\hat{\mu}_1(0)$. On the other hand, the probe dipole $\hat{\mu}_2(t)$ depends on the pump-probe time delay *t*. Rotational dynamics are manifested as the time dependence of the angle ϕ_2 between the two transition dipoles $\hat{\mu}_1(0)$ and $\hat{\mu}_2(t)$. The quantity δ denotes the angle between the pump polarization and the probe polarization, with $\delta = 0$ indicating a parallel polarization configuration and $\delta = \pi/2$ indicating a perpendicular polarization configuration. The remaining angles will be averaged out in the derivation of the time dependent rotational anisotropy.

Figure 1 shows these vectors as well as definitions of the relevant angles among them. The angle δ between the two space-fixed polarization vectors of the pump and the probe lasers is an experimentally controllable parameter; the condition $\delta = 0$ signifies a parallel polarization configuration, while $\delta = \pi/2$ represents a perpendicular polarization configuration. The angle $\phi_2(t)$ between the two molecule-fixed vectors, i.e., the pump dipole $\hat{\mu}_1(0)$ and the probe dipole $\hat{\mu}_2(t)$, contains information about the rotational dynamics of interest. The remaining angles will be averaged out in the course of the derivation.

Since we have assumed that the *m* pump transition dipoles are all parallel to each other, the probability for the *m*-photon pump transition is expected to be proportional to $|\hat{\mu}_1(0) \cdot \hat{\epsilon}_1|^{2m}$ under nonsaturated conditions. A similar expression can be obtained for the probe transition probability.

Thus, if none of the transitions is saturated, we can express the time dependent signal for an m-photon pump and n-photon probe as the following ensemble average:

$$\begin{aligned} I_\delta(t) &= A(t)\langle|\hat{\mu}_1(0)\cdot\hat{\epsilon}_1|^{2m}|\hat{\mu}_2(t)\cdot\hat{\epsilon}_2|^{2n}\rangle_{\theta_1,\phi_1,\chi_1,\mathbf{j}} \\ &= A(t)\langle\cos^{2m}\theta_1\cos^{2n}\theta_2\rangle_{\theta_1,\phi_1,\chi_1,\mathbf{j}} \\ &= A(t)\left\langle\frac{1}{8\pi^2}\int_0^{\pi}\sin\theta_1 d\theta_1\int_0^{2\pi}d\phi_1\right. \\ &\quad\left.\times\int_0^{2\pi}d\chi_1\cos^{2m}\theta_1\cos^{2n}\theta_2\right\rangle_{\mathbf{j}}, \end{aligned} \tag{1}$$

where $A(t)$ represents the isotropic contribution to the signal and therefore does not depend on rotational anisotropy.[30–32] The subscript δ in $I_\delta(t)$ signifies the dependence of signal on the polarization configuration. It is this dependence that is typically sought in an anisotropy measurement.

The averages in (1) take into consideration the contributions from individual molecules and can be viewed essentially as a summation (or rather average) over a collection of individual molecules. Since the transition dipoles $\hat{\mu}_1(0)$ and $\hat{\mu}_2(t=0)$ (at time zero) are molecule-fixed vectors, they are determined completely if the molecular orientation is specified. The molecular orientation can be characterized, for instance, by the three angles θ_1, ϕ_1, χ_1 defined in Fig. 1. Here, θ_1 and ϕ_1 define the orientation of $\hat{\mu}_1(0)$ while χ_1 specifies rotation about $\hat{\mu}_1(0)$. The time evolution of the probe dipole $\hat{\mu}_2(t)$ is governed by the angular momentum $\mathbf{j}$ of the species being probed. The quantity $\mathbf{j}$ is conserved at least until collisions take place; this is a relatively long period of time in a rarefied gas phase experiment like those in this study. The average over the molecules can be replaced with the average over θ_1, ϕ_1, χ_1 and $\mathbf{j}$ so long as the population of the species being pumped with orientation θ_1, ϕ_1, χ_1 and the population of the species being probed with angular momentum $\mathbf{j}$ are used as the weights for the average.

With the definition of vectors and angles in Fig. 1, the second equality in (1) is straightforward and needs no further explanation. The third equality in (1) expressed the average over θ_1, ϕ_1, χ_1 explicitly. As mentioned previously, these angles specify the orientation of the species being pumped. If there is no preferential orientation for the species being pumped initially, we should then take a uniformly weighted average over all possible orientations as in the third equality of expression (1). We now evaluate the 3D integral in (1) and leave the remaining average over $\mathbf{j}$ to later discussion.

In order to express θ_2 in terms of the angles θ_1, ϕ_1 and χ_1, we will make use of the following trigonometric identities:[33]

$$\begin{aligned} &\cos\theta_2 = \cos\gamma\cos\phi_2 + \sin\gamma\sin\phi_2\cos\chi_1, \\ &\cos\gamma = \cos\delta\cos\theta_1 + \sin\delta\sin\theta_1\cos\phi_1, \end{aligned} \tag{2}$$

where the angle γ is defined in Fig. 1. For simplicity, we will deal with two specific cases in the following, i.e., parallel ($\delta=0$) and perpendicular ($\delta=\pi/2$) polarization configurations. For $\delta=0$, we have from (2),

$$\begin{aligned} &\gamma = \theta_1 \\ &\cos\theta_2 = \cos\theta_1\cos\phi_2 + \sin\theta_1\sin\phi_2\cos\chi_1. \end{aligned} \tag{3}$$

Substituting (3) in (1), we obtain[34]

$$\begin{aligned} I_\parallel(t) &= \left\langle\frac{A(t)}{8\pi^2}\int\int\int\cos^{2m}\theta_1(\cos\theta_1\cos\phi_2\right. \\ &\quad\left.+\sin\theta_1\sin\phi_2\cos\chi_1)^{2n}\sin\theta_1 d\theta_1 d\phi_1 d\chi_1\right\rangle_{\mathbf{j}} \\ &= A(t)\,\frac{(-1)^{m+2n}n\pi\Gamma(2n)}{2^{2n}\Gamma(-m+n+1/2)\Gamma(m+n+3/2)} \\ &\quad\times\langle\sin^{2n}\phi_2 C_{2n}^{m-n+1/2}(i\,|\cot\phi_2|)\rangle_{\mathbf{j}}, \end{aligned} \tag{4}$$

where $\Gamma(x)$ and $C_k^\alpha(x)$ denote the gamma and the Gegenbauer functions, respectively.[33] Similarly, for perpendicular polarization configuration, $\delta=\pi/2$ and thus we have from (2),

$$\begin{aligned} &\cos\theta_2 = \cos\gamma\cos\phi_2 + \sin\gamma\sin\phi_2\cos\chi_1, \\ &\cos\gamma = \sin\theta_1\cos\phi_1. \end{aligned} \tag{5}$$

Substituting (5) in (1), we get

$$\begin{aligned} I_\perp(t) &= \left\langle\frac{A(t)}{8\pi^2}\int\int\int\cos^{2m}\theta_1(\cos\gamma\cos\phi_2\right. \\ &\quad\left.+\sin\gamma\sin\phi_2\cos\chi_1)^{2n}\sin\theta_1 d\theta_1 d\phi_1 d\chi_1\right\rangle_{\mathbf{j}} \\ &= A(t)\,\frac{\Gamma(m+1/2)\Gamma(n+1/2)}{2\sqrt{\pi}\Gamma(m+n+3/2)} \\ &\quad\times\langle\cos^{2n}\phi_2\,{}_2F_1(m+1,-n;-\tan^2\phi_2)\rangle_{\mathbf{j}}, \end{aligned} \tag{6}$$

where ${}_2F_1(a,b;x)$ denotes the confluent hypergeometric function.[33] For the special case of $m=n=1$, expressions (4) and (6) reduce to

$$\begin{aligned} I_\parallel(t) &= \frac{A(t)}{15}\langle 2+\cos 2\phi_2\rangle_{\mathbf{j}}, \\ I_\perp(t) &= \frac{A(t)}{30}\langle 3-\cos 2\phi_2\rangle_{\mathbf{j}}. \end{aligned} \tag{7}$$

Thus the above expressions give rise to the well-known formulation for the rotational anisotropy,[26,30,31]

$$r(t) = \frac{I_\parallel(t)-I_\perp(t)}{I_\parallel(t)+2I_\perp(t)} = \frac{1}{10}\langle 1+3\cos 2\phi_2\rangle_{\mathbf{j}}. \tag{8}$$

For an m-photon pump and one-photon probe, we have

$$\begin{aligned} I_\parallel(t) &= 2A(t)\,\frac{3^m}{2m+1}\left[1+\frac{m}{2m+3}\langle 1+3\cos 2\phi_2\rangle_{\mathbf{j}}\right], \\ I_\perp(t) &= 2A(t)\,\frac{3^m}{2m+1}\left[1-\frac{1}{2}\frac{m}{2m+3}\langle 1+3\cos 2\phi_2\rangle_{\mathbf{j}}\right], \\ r(t) &= \frac{1}{2}\,\frac{m}{2m+3}\langle 1+3\cos 2\phi_2\rangle_{\mathbf{j}}. \end{aligned} \tag{9}$$

We derived the above expressions previously[19] by simply extending the Baskin and Zewail treatment.[32] The present

TABLE I. Anisotropy formulae for multiphoton pump and probe. Formulae for rotational anisotropy $r(t)$ as well as signal intensities for parallel ($I_\parallel$) and perpendicular ($I_\perp$) polarization configurations are derived for specific cases of *m*-photon pump and *n*-photon probe based on the procedure outlined in Sec. II A. The quantity ϕ_2 denotes the angle between the pump transition dipole $\hat{\mu}_1(0)$ at time zero and the probe transition dipole $\hat{\mu}_2(t)$ at an arbitrary time delay *t*. The average over **j** has not been carried out explicitly. Specific examples of such averages are given in Sec. II A. The symbol $A(t)$ in the $I_\parallel$ and $I_\perp$ expressions is a proportional constant that does not depend on the anisotropy. Notice the symmetry between *m* and *n*. Also notice that when both pump and probe are multiphoton transitions, the $r(t)$ expressions become complicated (see text). In contrast, so long as either the pump or the probe is a one-photon transition, $r(t)$ can be expressed as a simple multiplication factor times $\langle 1+3\cos 2\phi_2\rangle_{\mathbf{j}}$.

	$n=1$	$n=2$	$n=3$
$m=1$	$I_\parallel=\frac{A(t)}{15}\langle 2+\cos 2\phi_2\rangle_{\mathbf{j}}$	$I_\parallel=\frac{A(t)}{35}\langle 3+2\cos 2\phi_2\rangle_{\mathbf{j}}$	$I_\parallel=\frac{A(t)}{63}\langle 4+3\cos 2\phi_2\rangle_{\mathbf{j}}$
	$I_\perp=\frac{A(t)}{30}\langle 3-\cos 2\phi_2\rangle_{\mathbf{j}}$	$I_\perp=\frac{A(t)}{35}\langle 2-\cos 2\phi_2\rangle_{\mathbf{j}}$	$I_\perp=\frac{A(t)}{126}\langle 5-3\cos 2\phi_2\rangle_{\mathbf{j}}$
	$r(t)=\frac{1}{10}\langle 1+3\cos 2\phi_2\rangle_{\mathbf{j}}$	$r(t)=\frac{1}{7}\langle 1+3\cos 2\phi_2\rangle_{\mathbf{j}}$	$r(t)=\frac{1}{6}\langle 1+3\cos 2\phi_2\rangle_{\mathbf{j}}$
$m=2$	$I_\parallel=\frac{A(t)}{35}\langle 3+2\cos 2\phi_2\rangle_{\mathbf{j}}$	$I_\parallel=\frac{A(t)}{315}\langle 18+16\cos 2\phi_2+\cos 4\phi_2\rangle_{\mathbf{j}}$	$I_\parallel=\frac{A(t)}{231}\langle 10+10\cos 2\phi_2+\cos 4\phi_2\rangle_{\mathbf{j}}$
	$I_\perp=\frac{A(t)}{35}\langle 2-\cos 2\phi_2\rangle_{\mathbf{j}}$	$I_\parallel=\frac{A(t)}{840}\langle 27-20\cos 2\phi_2+\cos 4\phi_2\rangle_{\mathbf{j}}$	$I_\perp=\frac{A(t)}{1848}\langle 41-36\cos 2\phi_2+3\cos 4\phi_2\rangle_{\mathbf{j}}$
	$r(t)=\frac{1}{7}\langle 1+3\cos 2\phi_2\rangle_{\mathbf{j}}$	$r(t)=\frac{\langle 63+188\cos 2\phi_2+5\cos 4\phi_2\rangle_{\mathbf{j}}}{2\langle 153+4\cos 2\phi_2+7\cos 4\phi_2\rangle_{\mathbf{j}}}$	$r(t)=\frac{\langle 39+116\cos 2\phi_2+5\cos 4\phi_2\rangle_{\mathbf{j}}}{2\langle 81+4\cos 2\phi_2+7\cos 4\phi_2\rangle_{\mathbf{j}}}$
$m=3$	$I_\parallel=\frac{A(t)}{63}\langle 4+3\cos 2\phi_2\rangle_{\mathbf{j}}$	$I_\parallel=\frac{A(t)}{231}\langle 10+10\cos 2\phi_2+\cos 4\phi_2\rangle_{\mathbf{j}}$	$I_\parallel=\frac{A(t)}{6006}\langle 200+225\cos 2\phi_2+36\cos 4\phi_2+\cos 6\phi_2\rangle_{\mathbf{j}}$
	$I_\perp=\frac{A(t)}{126}\langle 5-3\cos 2\phi_2\rangle_{\mathbf{j}}$	$I_\perp=\frac{A(t)}{1848}\langle 41-36\cos 2\phi_2+3\cos 4\phi_2\rangle_{\mathbf{j}}$	$I_\perp=\frac{5A(t)}{96096}\langle -294+303\cos 2\phi_2-42\cos 4\phi_2+\cos 6\phi_2\rangle_{\mathbf{j}}$
	$r(t)=\frac{1}{6}\langle 1+3\cos 2\phi_2\rangle_{\mathbf{j}}$	$r(t)=\frac{\langle 39+116\cos 2\phi_2+5\cos 4\phi_2\rangle_{\mathbf{j}}}{2\langle 81+4\cos 2\phi_2+7\cos 4\phi_2\rangle_{\mathbf{j}}}$	$r(t)=\frac{\langle 1730+5115\cos 2\phi_2+366\cos 4\phi_2+21\cos 6\phi_2\rangle_{\mathbf{j}}}{2\langle 3070+285\cos 2\phi_2+498\cos 4\phi_2+3\cos 6\phi_2\rangle_{\mathbf{j}}}$

formulation allows us to deal with multiphoton probe also. For a one-photon pump and *n*-photon probe, we have

$$I_\parallel(t)=2A(t)\,\frac{3^n}{2n+1}\left[1+\frac{n}{2n+3}\langle 1+3\cos 2\phi_2\rangle_{\mathbf{j}}\right],$$

$$I_\perp(t)=2A(t)\,\frac{3^n}{2n+1}\left[1-\frac{1}{2}\,\frac{n}{2n+3}\langle 1+3\cos 2\phi_2\rangle_{\mathbf{j}}\right],$$

$$r(t)=\frac{1}{2}\,\frac{n}{2n+3}\langle 1+3\cos 2\phi_2\rangle_{\mathbf{j}}. \tag{10}$$

By comparing (9) and (10), we realize that the two are essentially the same. The only difference is that every occurrence of *m* in (9) is now replaced with *n* in (10). Thus if either the pump or the probe transition is a one-photon process, a very simple expression can be obtained for the rotational anisotropy. The quantity $r(t)$ is found to be a constant multiplied by $\langle 1+3\cos\phi_2\rangle_j$ in this case.

However, when both pump and probe transitions are multiphoton processes, we can no longer obtain such a simple expression for the rotational anisotropy. Presented in Table I are the expressions of $I_\parallel$, $I_\perp$ and $r(t)$ for the cases when *m* and *n* each varies from 1 to 3. Taking the expressions for $I_\parallel$ and $I_\perp$ from the table, we find that for the case of multiphoton pump and multiphoton probe, $I_\parallel+2I_\perp$ contains expressions involving the angle ϕ_2. Since ϕ_2 depends on the angular momentum **j** of the species being probed, as we will see in the ongoing discussions, $I_\parallel+2I_\perp$ is no longer isotropic. Therefore, the rotational anisotropy as defined in (8) is not as meaningful a quantity for these cases as it was when Gordon first proposed it.[26] In fact, no linear combination or simple and meaningful nonlinear functions (at least the ones that we have examined) of $I_\parallel$ and $I_\perp$ can be isotropic if both the pump and the probe are multiphoton transitions.

The symmetry between *m* and *n* is also apparent in Table I although it is not immediately obvious from the expressions (4) and (6). This symmetry can be understood from examination of the integration in Eq. (1). The integration (or average) over θ_1, ϕ_1 and χ_1 in (1) can be transformed into an integration (or average) over θ_2, ϕ_2 and χ_2 with the value of the integration unchanged. This is because there is no difference between integration over all possible orientations with θ_1, ϕ_1 and χ_1 as integration variables and integration over all possible orientations with θ_2, ϕ_2 and χ_2 as integration variables.

Further averaging over the angular momentum **j** in the above expressions can be carried out by following the procedure given by Baskin and Zewail.[32] However, for completeness, we will give an outline of the procedure with a particular emphasis on the case of multiphoton pump and probe. The following derivation will be limited to the case of a symmetric top. To fully specify **j** with respect to a symmetric top, one needs to specify its magnitude *j*, the angle θ between **j** and the figure axis of the top and the angle of rotation ψ_0 around the figure axis at time zero. With these three quantities specified, the classical motion of the top can be determined completely. As is well known, the top motion is a composite of two different types of rotation: the nutation of the figure axis about **j** at a rate $\omega_n=j/i_\perp$ and the rotation

of the top about its figure axis at a rate $\omega_r = j\cos\theta(1/i_\parallel - 1/i_\perp)$, where $i_\parallel$ and $i_\perp$ denote, respectively, the moments of inertia of the molecule about its top axis and about any axis perpendicular to it.[35] Thus the equations of motion for the unit vectors along the top axes x, y and z become[32]

$$\hat{x}(t) = [\cos(\psi_0+\omega_r t)\cos\omega_n t - \cos\theta \times \sin(\psi_0+\omega_r t)\sin\omega_n t]\hat{X} + [\cos(\psi_0+\omega_r t) \times \sin\omega_n t + \cos\theta\sin(\psi_0+\omega_r t)\cos\omega_n t]\hat{Y} + \sin\theta\sin(\psi_0+\omega_r t)\hat{Z}, \quad (11a)$$

$$\hat{y}(t) = [-\sin(\psi_0+\omega_r t)\cos\omega_n t - \cos\theta \times \cos(\psi_0+\omega_r t)\sin\omega_n t]\hat{X} + [-\sin(\psi_0+\omega_r t) \times \sin\omega_n t + \cos\theta\cos(\psi_0+\omega_r t)\cos\omega_n t]\hat{Y} + \sin\theta\cos(\psi_0+\omega_r t)\hat{Z}, \quad (11b)$$

$$\hat{z}(t) = \sin\theta\sin\omega_n t\hat{X} - \sin\theta\cos\omega_n t\hat{Y} + \cos\theta\hat{Z}, \quad (11c)$$

where z denotes the figure axis of the top and $\hat{X}$, $\hat{Y}$ and $\hat{Z}$ are the unit vectors along the space-fixed axes of the coordinate system.

Knowing the time evolution of the unit vectors along the top axes, the time evolution of an arbitrary vector can be predicted so long as its resolution in terms of the top unit vectors $\hat{x}$, $\hat{y}$ and $\hat{z}$ is known. To illustrate this point, we will evaluate the **j** averages in Eq. (9) for two simple cases, one of which is of interest to the present study. First, the pump and probe dipoles are parallel to each other and to the figure axis at time zero. We will use subscript $(\parallel,\parallel)$ to denote this case. Second, the pump and probe dipoles are perpendicular to each other at time zero with one of them parallel to the figure axis. We will use $(\parallel,\perp)$ to denote this latter case. For both cases, the molecule being probed is assumed to be linear. Thus $\theta=\pi/2$ becomes a very good approximation because in this case if the electronic and spin angular momenta can be neglected, the total angular momentum **j** is essentially the rotational angular momentum, which is perpendicular to the linear molecular axis.[36]

For the $(\parallel,\parallel)$ case, both the pump dipole $\hat{\mu}_1$ and the probe dipole $\hat{\mu}_2$ are parallel to the molecule-fixed z-axis (figure axis). Thus $\hat{\mu}_1(0)=\hat{z}(0)$ and $\hat{\mu}_2(t)=\hat{z}(t)$. Using Eq. (11) and taking into consideration $\theta=\pi/2$, this gives

$$\cos\phi_2 = \hat{\mu}_1(0)\cdot\hat{\mu}_2(t) = \hat{z}(0)\cdot\hat{z}(t) = \cos\omega_n t, \quad (12)$$

or $\phi_2=\omega_n t$. Therefore the rotational anisotropy in Eq. (9) reduces to

$$r_{\parallel,\parallel}(t) = \frac{1}{2}\frac{m}{2m+3}\langle 1+3\cos 2\phi_2\rangle_{\mathbf{j}} = \frac{1}{2}\frac{m}{2m+3}\langle 1+3\cos 2\omega_n t\rangle_{j,\theta,\psi_0} = \frac{1}{2}\frac{m}{2m+3}\left[1+3\frac{\Sigma_j P_j\cos 2\omega_n t}{\Sigma_j P_j}\right]. \quad (13)$$

Since $\omega_n t$ depends on j but not on θ or ψ_0, only the j average is explicitly carried out in the last step. The quantity P_j denotes the rotational distribution of the species probed.

Similarly, for the $(\parallel,\perp)$ case, without loss of generality, we can let $\hat{\mu}_1(0)=\hat{z}(0)$ and $\hat{\mu}_2(t)=\hat{x}(t)$. Then we obtain

$$\cos\phi_2 = \hat{\mu}_1(0)\cdot\hat{\mu}_2(t) = \hat{z}(0)\cdot\hat{x}(t) = -\cos(\psi_0+\omega_r t)\sin\omega_n t. \quad (14)$$

When this result is substituted into the rotational anisotropy expression in (9), we find

$$r_{\parallel,\perp}(t) = \frac{1}{2}\frac{m}{2m+3}\langle 1+3\cos 2\phi_2\rangle_{\mathbf{j}} = \frac{1}{2}\frac{m}{2m+3}\langle -2+6\cos^2(\psi_0+\omega_r t)\sin^2\omega_n t\rangle_{j,\theta,\psi_0} = -\frac{1}{4}\frac{m}{2m+3}\langle 1+3\cos 2\omega_n t\rangle_j = -\frac{1}{4}\frac{m}{2m+3}\left[1+3\frac{\Sigma_j P_j\cos 2\omega_n t}{\Sigma_j P_j}\right], \quad (15)$$

where the average over ψ_0 is assumed to be uniformly weighted. After such averaging, the only ψ_0 dependent factor $\cos^2(\psi_0+\omega_r t)$ becomes 1/2. Notice that the anisotropy in (15) is exactly $-1/2$ times that in (13). Similar **j** averages can be carried out for other more complicated cases.

Before we leave this subsection, it is perhaps worthwhile to mention the applicability of the above formulation. The above expressions should be valid if the signal is proportional to the total population transferred by the probe transition.[32] Detection schemes such as transient absorption, fluorescence depletion (this study) or multiphoton ionization obviously fall into this category. However, further complications arise if, for instance, the polarized fluorescence from the terminal level of the pump/probe transition sequence is taken as the signal. For this case, one must consider the alignment created in the pump/probe steps instead of just the pump step alone. A formulation for this case has been given by Baskin and Zewail[32] for the one-photon pump and one-photon probe. Extension of this formulation to the cases of multiphoton pump and probe is currently under consideration.

B. Three-body mechanics

As far as the photoinduced molecular detachment processes in this study are concerned, the penta-atomic molecule CH_2I_2 can be treated as a triatomic with the CH_2 moiety being viewed as a pseudoatom. This subsection deals with the kinematics of such a three-particle system using the laws of classical mechanics. The purpose is to see how bond breaking and formation affect the motion of the individual particles, knowledge of which allows an analysis of the angular momenta of the subsystems. This analysis will be useful to the discussion of the possible mechanisms in Sec. IV D. In the following treatment, we will assume that the bonds are rigid and that there is no translation or rotation of the system as a whole. Excess energy deposited to dissociate a bond is assumed to be manifested as a force acting along

the direction of the bond (i.e., axial recoil). Therefore, it is sufficient to consider only the motion of the atoms on the triatomic plane.

To illustrate the general idea of the treatment, we will consider a specific bonding arrangement, i.e., atom 1 is initially bonded to atom 2 and atom 2 to atom 3 (e.g., the CH_2 pseudoatom to the two I atoms of CH_2I_2). Let m_i, (x_i, y_i) and (v_{xi}, v_{yi}) be the mass, current position and velocity of atom i, respectively. At an infinitesimal time δt later, changes of the atomic positions can be determined trivially using $\delta x_1 = v_{x1}\delta t$, etc. The changes in the atomic velocities, on the other hand, can be determined by the following set of simultaneous equations:

$$\delta P_x = m_1\delta v_{x1} + m_2\delta v_{x2} + m_3\delta v_{x3} = 0, \tag{16a}$$

$$\delta P_y = m_1\delta v_{y1} + m_2\delta v_{y2} + m_3\delta v_{y3} = 0, \tag{16b}$$

$$\delta J_z = m_1(x_1\delta v_{y1} - y_1\delta v_{x1}) + m_2(x_2\delta v_{y2} - y_2\delta v_{x2}) + m_3(x_3\delta v_{y3} - y_3\delta v_{x3}) = 0, \tag{16c}$$

$$\delta T = m_1(v_{x1}\delta v_{x1} + v_{y1}\delta v_{y1}) + m_2(v_{x2}\delta v_{x2} + v_{y2}\delta v_{y2}) + m_3(v_{x3}\delta v_{x3} + v_{y3}\delta v_{y3}) = 0, \tag{16d}$$

$$\tfrac{1}{2}\delta\frac{dr_{12}^2}{dt} = [(v_{x1} - v_{x2})^2 + (v_{y1} - v_{y2})^2]\delta t + (x_1 - x_2) \times (\delta v_{x1} - \delta v_{x2}) + (y_1 - y_2)(\delta v_{y1} - \delta v_{y2}) = 0, \tag{16e}$$

$$\tfrac{1}{2}\delta\frac{dr_{23}^2}{dt} = [(v_{x2} - v_{x3})^2 + (v_{y2} - v_{y3})^2]\delta t + (x_2 - x_3) \times (\delta v_{x2} - \delta v_{x3}) + (y_2 - y_3)(\delta v_{y2} - \delta v_{y3}) = 0, \tag{16f}$$

where Eqs. (16a)–(16d) are essentially the conservation laws of momentum, angular momentum and kinetic energy. Equations (16e) and (16f) are imposed by the rigid bonds between atoms 1 and 2 and between atoms 2 and 3, respectively. These equations govern the free propagation of the triatomic system.

We now consider the situation of a bond breaking event, specifically breaking of the 1-2 bond with an excess energy E. We will assume that the bond breaking event is instantaneous, so there is no change in the position of each atom before and after the breaking. But there will be abrupt changes in the velocities of the atoms, which can be obtained by solving the following simultaneous equations:

$$\delta P_x = m_1\delta v_{x1} + m_2\delta v_{x2} + m_3\delta v_{x3} = 0, \tag{17a}$$

$$\delta P_y = m_1\delta v_{y1} + m_2\delta v_{y2} + m_3\delta v_{y3} = 0, \tag{17b}$$

$$\delta J_z = m_1(x_1\delta v_{y1} - y_1\delta v_{x1}) + m_2(x_2\delta v_{y2} - y_2\delta v_{x2}) + m_3(x_3\delta v_{y3} - y_3\delta v_{x3}) = 0, \tag{17c}$$

$$\delta T = m_1(v_{x1}\delta v_{x1} + v_{y1}\delta v_{y1}) + m_2(v_{x2}\delta v_{x2} + v_{y2}\delta v_{y2}) + m_3(v_{x3}\delta v_{x3} + v_{y3}\delta v_{y3}) = E, \tag{17d}$$

$$\frac{\delta v_{x1}}{\delta v_{y1}} = \frac{x_1 - x_2}{y_1 - y_2}, \tag{17e}$$

$$\tfrac{1}{2}\delta\frac{dr_{23}^2}{dt} = (x_2 - x_3)(\delta v_{x2} - \delta v_{x3}) + (y_2 - y_3)(\delta v_{y2} - \delta v_{y3}) = 0, \tag{17f}$$

where Eqs. (17a)–(17c) are identical to those in (16). Equation (17e) reflects the restriction that bond breaking results in axial recoil. Similar free propagation and bond breaking equations can also be obtained for other bonding arrangements and bond formation and bond breaking processes. With these equations, the motion of the atoms can be predicted and mechanical quantities such as the angular momentum of the subsystems (fragments) can be obtained readily.

III. EXPERIMENTAL RESULTS

Since a detailed description of the experimental apparatus has been given in paper I,[1] here we will give only a brief account of the experimental setup and conditions. The experiments employ two femtosecond laser beams (~50 fs pulsewidths) with one beam having its wavelength centered around 312 (pump) and the other around 624 nm (probe). Pump and probe beams were collinearly overlapped and focused into a quartz sample cell using a lens of 200 mm focal length. Fluorescence from the product molecules was focused into a spectrometer for detection.

CH_2I_2 was introduced to a quartz cell and dissolved gases removed by several freeze-pump-thaw cycles to 10^{-5} Torr at liquid nitrogen temperature. Dehydrated sodium thiosulfate was also placed in the cell to scavenge iodine molecules to ensure only nascent I_2 photofragments were present. Experiments were conducted at room temperature. Spectra were taken using the 312 nm laser only and the wavelength scale was calibrated with a Hg lamp using the known emission lines of Hg atoms.[37] The resultant dispersed fluorescence spectrum is presented in Fig. 2.

The dynamics associated with the strong fluorescence features between 300 and 350 nm has been investigated in paper I.[1] In this study, we will focus on the dynamics associated with the weak fluorescence features in the 260–290 nm region. As has been mentioned in paper I,[1] the strong fluorescence only accounts for photodissociation channels with less than 0.01 quantum yield. The quantum yield for the weak fluorescence can be estimated to be about one order of magnitude less than the stronger one, or less than 0.001. The time-resolved experiments which we will present in the following use only a fraction (~10 nm) of the weak spectrum in the 260–290 nm region as signal. Additionally, since the dynamic information is contained in the depletion of the weak fluorescence signal, extra effort and caution are necessary to acquire meaningful time-resolved transients.

To obtain time-resolved data, the probe pulse at 624 nm was used to deplete the population in the fluorescent state and transients were recorded as a function of fluorescence signal versus time delay between the pump and probe pulses. At each pump-probe time delay, the signal was collected for 10 laser shots; laser pulses with intensity more than one stan-

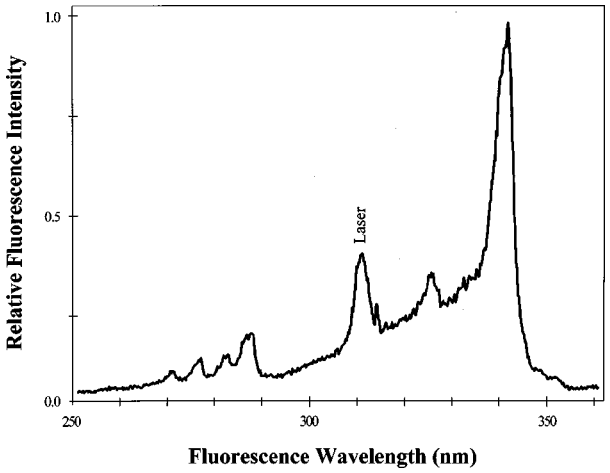

FIG. 2. Fluorescence spectrum obtained from multiphoton excitation of CH_2I_2 at 312 nm. The spectrum was acquired by dispersing the fluorescence generated from excitation of the neat vapor of room temperature CH_2I_2. The excitation source is a focused ($f=200$ mm) femtosecond laser beam (~ 10 μJ/pulse) with a central wavelength at 312 nm. The spectrum was calibrated using known emission lines of a Hg lamp.

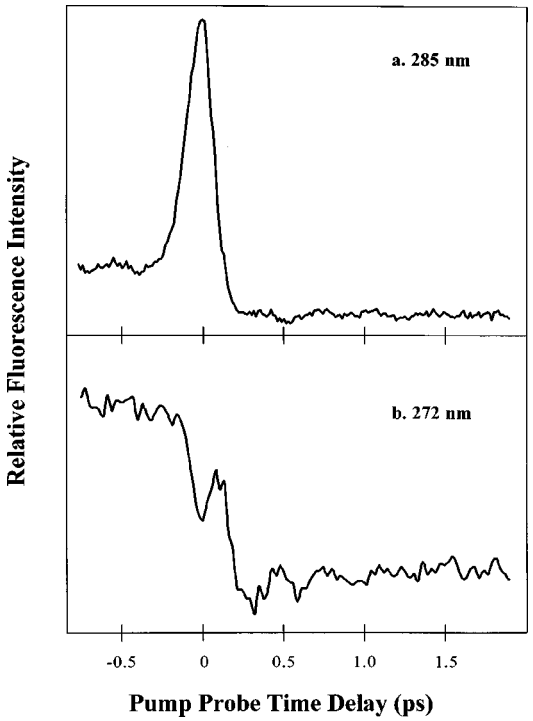

FIG. 3. Time-resolved transients for CH_2I_2. The transients were obtained by a time-resolved femtosecond pump-probe scheme. The pump pulses have a central wavelength at 312 and the probe pulses are centered at 624 nm. The polarization of the pump beam is parallel to that of the probe beam. Both the pump and the probe pulses have temporal width ~ 50 fs. The figure shows time-resolved data obtained by selective detection of the fluorescence signal at 285 nm [shown in panel (a)] and at 272 nm [shown in panel (b)]. Both transients show signatures of vibrational coherence. However, the 285 nm transient exhibits a large time zero spike.

dard deviation from the mean were discarded. Typical transients contain data from 200 different time delays and are averages of 100 scans. Figures 3(a) and 3(b) show the time-resolved transients for CH_2I_2 taken by collecting fluorescence signal at 285 and 272 nm, respectively. The dynamics observed for 285 nm detection are very similar to those found when detecting the $D' \rightarrow A'$ transition (see paper I).[1] However, the 272 transient is strikingly different from the 285 nm transient; the former does not show the time zero feature. As we will show, absence of the time zero spike in the 272 nm transient allows rotational anisotropy to be measured.

Both transients in Fig. 3 were obtained with the pump and probe polarization vectors aligned parallel to each other. Perpendicular transients, i.e., transients taken with the pump and probe polarization perpendicular to each other, were also obtained for CH_2I_2 at both 285 and 272 nm. Although there is no discernible difference between the parallel and perpendicular transients collected at 285 nm, significant difference exists between the parallel and perpendicular 272 nm transients, as depicted in Fig. 4. The data in Fig. 4 were collected by setting the polarization of the pump (312 nm) pulses normal to the optical table; the polarization of the probe (624 nm) pulses was then aligned either parallel or perpendicular to that of the pump.

The time dependent rotational anisotropy is extracted from the data using the formula,[26]

$$r(t)=\frac{I_{\parallel}-I_{\perp}}{I_{\parallel}+2I_{\perp}}, \tag{18}$$

and the ''isotropic signal,'' which reflects the pure vibrational contribution, can be isolated using the following formula,

$$I_{\text{isotropic}}=I_{\parallel}+2I_{\perp}. \tag{19}$$

In Eqs. (18) and (19), $I_{\parallel}$ is the fluorescence intensity obtained when the pump and probe lasers are polarized parallel to each other and $I_{\perp}$ the intensity when they are polarized perpendicularly. This separation of pure vibrational and pure rotational contributions from the observed experimental data allows us to study them without interference from each other.

Presented in Figs. 5(a) and 5(b) are the pure vibrational and pure rotational contributions derived from the 272 nm transients in Fig. 4. To obtain the experimental $r(t)$ and $I_{\text{isotropic}}$ curves shown in Fig. 5, the average fluorescence intensity at negative time delays (probe earlier than pump) was subtracted from the parallel and perpendicular transients, and proper normalization of these transients at long time delay to their respective asymptotic limits was performed. The observed data were not manipulated in any other way before evaluating $r(t)$.

IV. DISCUSSIONS

A. Vibrational analysis

The isotropic transient shown in Fig. 5(a) clearly exhibits its oscillative variation in $I_{\text{isotropic}}$ at positive time delays. This nearly sinusoidal variation can be interpreted as the signature of the coherent vibrational motion imparted to the nascent I_2 fragments during the dissociation process. The observed vibrational coherence in the I_2 fragment implies that

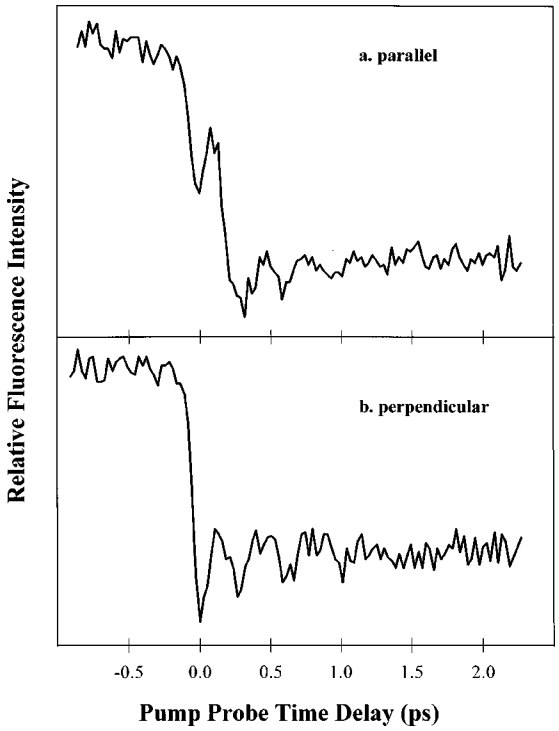

FIG. 4. Time-resolved transients of CH_2I_2 collected at 272 nm. Panel (a) of the figure shows a transient obtained for a parallel polarization configuration between the pump and probe beams while panel (b) shows a transient for perpendicular polarization configuration. The difference between the two transients clearly indicates rotational anisotropy in the I_2 product. The anisotropy decays within ~500 fs of the pump excitation. Notice that for the perpendicular polarization configuration, the depletion is greater near time zero than that for the parallel polarization configuration.

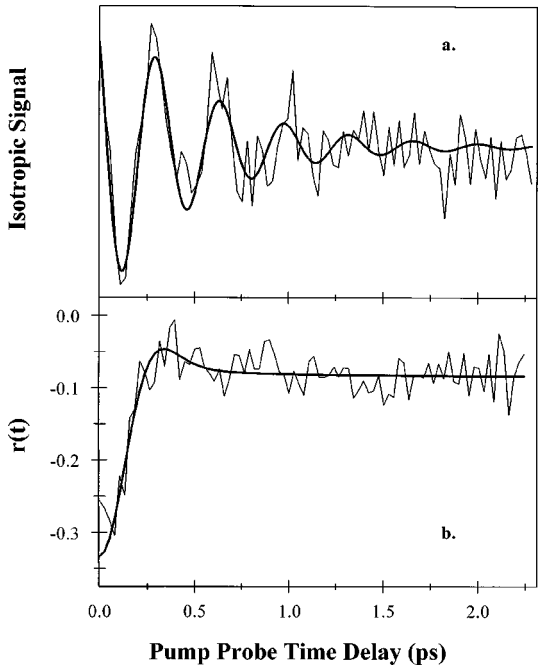

FIG. 5. Separation of pure vibration and pure rotation contributions to the signal. The thinner traces in both panels (a) and (b) present, respectively, the pure vibrational contribution as given by the isotropic signal $I_{\parallel}+2I_{\perp}$ and the pure rotational contribution as given by the time dependent rotational anisotropy $r(t)$ [see Eq. (18)]. Both the isotropic signal and the rotational anisotropy are derived from the original experimental data given in Fig. 4. The thicker lines show least-squares fits to the pure vibrational and pure rotational contributions.

the I_2 elimination process is concerted, i.e., I—I bond formation and the two C—I bond breakages happen in a single kinetic step.[1,17–19]

To obtain quantitative information about the vibrational coherence, we have modeled the isotropic data in Fig. 5(a) using the following damped sinusoidal expression:

$$I_{\text{isotropic}}=A+Be^{-t/\tau}\cos(\omega t+\phi), \tag{20}$$

where τ denotes the effective coherence dephasing constant, ω the vibrational frequency and ϕ a phase factor. The quantities A and B are constants dependent upon specific experimental conditions, such as detection efficiency. The exponential factor accounts for the effective dephasing of the vibrational coherence whereas the cosine factor describes the signature of the vibrational motion. Least-squares fit of the experimental isotropic data in Fig. 5(a) using the functional form of (20) gives rise to the following parameters: $\tau=501\pm82$ fs, $\omega=98\pm2$ cm^{-1} and $\phi=51°\pm6°$. The fitted result is shown in Fig. 5(a) as a solid curve.

These fitted parameters, especially the vibrational frequency, provide clues to the identity of the fragment being probed and the electronic identity of its fluorescent state. First of all, since most ion-pair states of I_2 have vibrational frequencies on the order of 100 cm^{-1}, there seems little doubt that the species being probed is the I_2 fragment. Second, because anharmonicity tends to reduce the effective vibrational frequency for higher-lying vibrational levels, the fitted vibrational frequency should provide a lower bound to the nominal vibrational frequency of the fluorescent state. This serves as a convenient criterion for eliminating as the fluorescent state those I_2 states that have vibrational frequencies smaller than 98 cm^{-1}.

There are several known emission systems of I_2 that fall into the 260–290 nm spectral region, notably the $F0_u^+ \rightarrow X0_g^+$,[38] $f0_g^+ \rightarrow A1_u$,[38] $f0_g^+ \rightarrow B''1_u$,[38] $f'0_g^+ \rightarrow B0_u^+$,[39] $G1_g \rightarrow A1_u$[38,40] and $g0_g^- \rightarrow 2431\ ^3\Pi_{0u}^-$[38,41] transitions. Since the vibrational frequencies of both the $F0_u^+$ (96.31) and the $f'0_g^+$ (96.98 cm^{-1}) states are smaller than the fitted vibrational frequency of 98 cm^{-1}, they are quite unlikely to be responsible for the observed vibrational coherence based upon the above criterion, although similar features observed by Okabe *et al.*[21] and Fotakis *et al.*[20] have been tentatively assigned to the $F0_u^+ \rightarrow X0_g^+$ fluorescence of the nascent I_2 fragment. However, due to the sizable uncertainty (2 cm^{-1}) in the present determination of the vibrational frequency, the lower bound of 96 cm^{-1} does not permit us to eliminate the involvement of the $F0_u^+$ and the $f'0_g^+$ states unequivocally.

The remaining three upper states have quite similar vibrational frequencies, i.e., 104.14 for $f0_g^+$, 106.60 for $G1_g$ and 105.70 cm^{-1} for $g0_g^-$. Taking into consideration the anharmonicity constants of 0.2113, 0.2134, and 0.4900 cm^{-1} for the *f*, *G* and *g* states, respectively, we can estimate that a vibrational frequency of 98 cm^{-1} corresponds to vibrational levels 14, 19 and 7, respectively. Spectral analysis presented in paper I[1] indicated that the I_2 $f \rightarrow B$ fluorescence is partially responsible for the stronger emission band in the 290–345

nm region. Therefore, it is no surprise that certain spectral features in the 260–290 nm region are due to the I_2 $f \rightarrow A$ fluorescence. Although we can not determine the exact identity of the fluorescent state responsible for the vibrational coherence, the above analysis strongly suggests that the f state is responsible.

Since the I—I interatomic distance in the ground state of CH_2I_2 is rather close to the bond lengths in the f, g and G states of the I_2 molecule,[16,38,40,41] significant vibrational excitation in the I_2 fragment is not expected. However, because the HCH angle in ground-state CH_2I_2 differs significantly from the bond angle of CH_2 in the $\tilde{X}$ and $\tilde{b}$ states,[16,42] vibrational excitation should be expected in the CH_2 photofragment if CH_2 is produced in the $\tilde{X}$ or $\tilde{b}$ state. This could represent a significant amount of energy, especially when one considers the high vibrational frequencies of CH_2.

The vibrational coherence decays over a period of approximately 500 fs. Under the experimental conditions of this study, the mean collision time can be estimated to be approximately 100 ns. Clearly, intermolecular collisions can not be responsible for the observed dephasing of vibrational coherence. The vibrational anharmonicity can also cause vibrational dephasing and loss of coherence. Although this may be largely responsible for the observed dephasing, a simulation with this as the only mechanism yields a very wide vibrational distribution and a less satisfactory fitting result. This indicates that other dephasing mechanisms play a part.

The fitted vibrational phase factor, ϕ in Eq. (20), is found to be nonzero. The uncertainty in determining the value of this factor is significantly affected by the accuracy of experimental determination of time zero. We have made use of the fact that when collecting fluorescence at 340 nm, a large spike can be observed at time zero (see paper I[1]). The peak position of the spike can serve as a very good indication of where the actual time zero is located. With this, the time zero can be estimated to be within the resolution of the time scan, which is less than 30 fs. This accounts for about 10% of the ~300 fs vibrational period. Thus the uncertainty of the phase factor can be estimated to be about ~36°, i.e., ~10% of the phase of a full period, 360°. Thus even with this large error, the fitted phase factor $\phi = 51° \pm 36°$ for this molecular detachment channel is quite different from that obtained for the D' dissociation pathway in paper I. An induction period, while bond rearrangement takes place, is a possible explanation for the observed nonzero phase factor.

B. Rotational analysis

Examination of the data in Fig. 4 reveals that depletion immediately after time zero is more efficient when the pump and probe pulses are polarized perpendicular to each other than when they are parallel. This is a strong indication that the dipole of the probe transition is perpendicular to the dipole of the pump transition at time zero. The implication of this observation to the symmetry of the excited states of the parent and the I_2 fragment will be explored in Sec. IV E. It is also quite apparent from Fig. 4 that there is a considerable degree of anisotropy in the data, most of which vanishes during the first 500 fs after formation of the I_2 photodissociation product. The fast decay implies a high degree of rotational excitation in the I_2 fragment.

A quantitative analysis of the rotational dephasing can be performed on the pure rotational contribution presented in Fig. 5(b). A formulation of time-dependent rotational anisotropy for the case of one-photon pump and one-photon probe has been given by Baskin and Zewail[32] for a ($\parallel$,$\parallel$) transition case. Extension of the formulation to the ($\parallel$,$\perp$) case yields

$$r(t) = -\frac{1}{20}\left(1 + 3\frac{\Sigma_j P_j \cos 2\omega_n t}{\Sigma_j P_j}\right), \tag{21}$$

where the symbols are defined as in Sec. II A. However, analysis of the pure rotational contribution shown in Fig. 5(b) using this formulation failed to reproduce the experimental data in general and the observed $r(0)$ value in particular. One can see from Fig. 5(b) that the $r(t)$ value at time zero is close to -0.3, especially if one follows the trend of the experimental trace. This is different from the expected value of -0.2 for a situation where the pump and probe transition dipoles are perpendicular to each other. We find that this is due to the multiphoton nature of the pump transition. A three-photon pump transition would be expected to produce a greater degree of alignment than is expected for a one-photon transition because it produces a $(\cos\theta)^6$ distribution in the nascent products rather than a $(\cos\theta)^2$ distribution. This narrower initial alignment causes the dephasing of rotational anisotropy to appear faster than it really is.

In order to model time-dependent rotational anisotropy experiments in which the excitation is a multiphoton process, we have extended the existing treatment[32] for one-photon pump and one-photon probe in Sec. II. A summary of the model with specific application to the case of a three-photon pump and one-photon probe follows. For this case, if all the pump transition dipoles are aligned parallel to each other and the probe dipole is perpendicular to the pump dipole at time zero, we find from Eq. (15) that the rotational anisotropy can be expressed as[19]

$$r(t) = -\frac{1}{12}\left[1 + 3\frac{\Sigma_j P_j \cos 2\omega_n t}{\Sigma_j P_j}\right], \tag{22}$$

where the weighting factor P_j describes the rotational population of the I_2 fragment, in this case a Gaussian function given by

$$P_j = \frac{1}{\sqrt{\pi}\Delta j}\, e^{-(j - j_{\max})^2/(\Delta j)^2}, \tag{23}$$

and $\omega_n = 4\pi B j$ denotes the j-dependent nutational frequency of the fragment being probed. The quantity B represents the rotational constant of the I_2 fragment. It is obvious from Eq. (22) that $r(0) = -1/3$. The discrepancy between this value and the experimental value [see Fig. 5(b)] may be attributed to finite signal to noise ratio. A least-squares fit of the observed $r(t)$ data using the above formulae is presented in Fig. 5(b) as the solid curve. As guided by the fitted curve, the trend of the experimental trace is seen to approach the expected $-1/3$ value toward time zero. The fit gives rise to the following parameters: the center of the rotational distribution

TABLE II. Energetics for several dissociation channels of CH_2I_2. The table gives the minimum energies required to dissociate a ground-state CH_2I_2 molecule to produce CH_2 and I_2 fragments in several possible electronic states. The available energies are calculated based on a three-photon transition at 312 nm. The relevant spectroscopic and thermochemical data are taken from the literature (Refs. 4, 38, 40, and 41).

I_2 States	CH_2 states	Energy required (eV)	Available energy (eV)
	$\tilde{X}\ ^3B_1$	9.20	2.72
$f(^3\Pi_{0g}^+), g(0_g^-)$	$\tilde{a}\ ^1A_1$	9.59	2.33
	$\tilde{b}\ ^1B_1$	10.47	1.45
	$\tilde{X}\ ^3B_1$	9.27	2.65
$G(1_g)$	$\tilde{a}\ ^1A_1$	9.66	2.26
	$\tilde{b}\ ^1B_1$	10.54	1.38

of the I_2 fragment, $j_{max}=354\pm38$, and the $1/e$ width of the distribution, $\Delta j=509\pm52$. The interesting implications of this fitting result will be explored in the following discussions.

C. Energy partitioning

As the vibrational analysis in Sec. IV A indicates, the *f*, *g* or *G* state of I_2 is likely to be responsible for the observed vibrational coherence after excitation of CH_2I_2 at 312 nm. Thus the following discussion will consider only dissociation pathways leading to formation of these states. Since production of I_2 molecules in the *f*, *g* and *G* states from a thermal sample of CH_2I_2 requires minimum energies of 9.20, 9.20 and 9.27 eV, respectively,[4,38,40,41] at least three photons of 312 nm are needed in each case to supply the necessary energy. A four-photon excitation would provide 16 eV of energy, which is far above the ionization threshold of CH_2I_2, so we believe that a three-photon excitation is more likely. Power dependence results also support this conclusion.[1] In addition, the rotational anisotropy data are consistent with a three-photon pump excitation. The following analysis is therefore made assuming that the excitation is a three-photon process.

If a 12 eV excitation produces I_2 in the *f*, *g* and *G* states, only the three lowest electronic states of CH_2, i.e., $\tilde{X}(^3B_1)$ ($T_0=0.0$ eV), $\tilde{a}(^1A_1)$ ($T_0=0.39$ eV) and $\tilde{b}(^1B_1)$ ($T_0=1.27$ eV),[36] can be produced by the photodissociation process. Table II lists possible combinations of the I_2 and CH_2 states, each of which represents a distinct photodissociation channel of CH_2I_2. For each channel, Table II also gives the minimum energy required for the dissociation process and the remaining energy available for internal and kinetic energies of the photofragments.

As shown in paper I,[1] the multiphoton molecular detachment process of CH_2I_2 is extremely fast. Examination of the transients shown in Fig. 4 also indicates the promptness of the dissociation process; the depletion is essentially instantaneous within the time resolution of 50 fs. In fact, the quantitative analysis of the time zero spike for the 340 nm fluoresce as presented in paper I predicted a dissociation time of 47 fs, from which we can estimate the translational energy of the photofragments to be on the order of 1.3 eV.

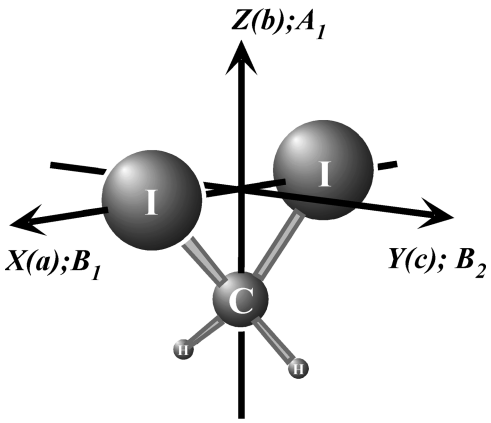

FIG. 6. A model of a CH_2I_2 molecule. The figure shows the principal (*X*, *Y* and *Z*) and rotational axes (*a*, *b* and *c*) as well as their transformation under the C_{2v} symmetry. Notice that the center of mass is very close to the center of the two I atoms.

It is useful in the following discussions to understand qualitatively how the rotational motion of the parent CH_2I_2 molecule is partitioned into the CH_2 and I_2 fragments. To facilitate these discussions, Fig. 6 shows a model of the CH_2I_2 molecule in the center-of-mass frame. Notice that the center of mass is essentially that of the I_2 fragment because the iodine atoms are considerably heavier than either carbon or hydrogen. Upon dissociation, most of the rotational energy of the parent CH_2I_2 about the *Z*-axis (*b*-axis), the symmetry axis of CH_2I_2, remains as rotational energy of the I_2 fragment because the moment of inertia of I_2 is significantly larger than that of CH_2. On the other hand, because the center of mass in CH_2I_2 is extremely close to the *X*-axis (*a*-axis), i.e., the line joining the two iodine atoms, rotational motion of CH_2I_2 about the *X*-axis will be manifested as translational motion of the CH_2 fragment. Similarly, rotational motion about the *Y*-axis (*c*-axis) will be partitioned into I_2 rotation and CH_2 translation upon dissociation. Thus the rotational motion of the parent CH_2I_2 essentially turns into translational motion of the CH_2 fragment and rotational motion of the I_2 fragment.

From fitting the observed rotational anisotropy data, we have determined the I_2 rotational distribution to be centered around $j_{max}=350$. With the known rotational constant of the fluorescent state(s), the average rotational energy of the product I_2 molecules can be estimated to be approximately 0.3 eV. From fitting the experimentally observed vibrational coherence data, the I_2 fragment has been found to contain only moderate vibrational excitation with an average vibrational quantum number of $v\approx14$ (for I_2 *f* state). With the vibrational frequency on the order of 100 cm^{-1}, we can estimate that the vibrational energy partitioned into the I_2 fragment is approximately 0.2 eV. This is smaller than the rotational energy, a rather uncommon situation. The small vibrational energy in the I_2 fragment can be attributed to the fact that the I—I distance in CH_2I_2 is very similar to that of I_2 ion-pair states and therefore little vibrational excitation is expected. Although we do not have a direct handle on how the rotational and vibrational energies are partitioned into the CH_2 fragment, based on previous discussions, we expect that

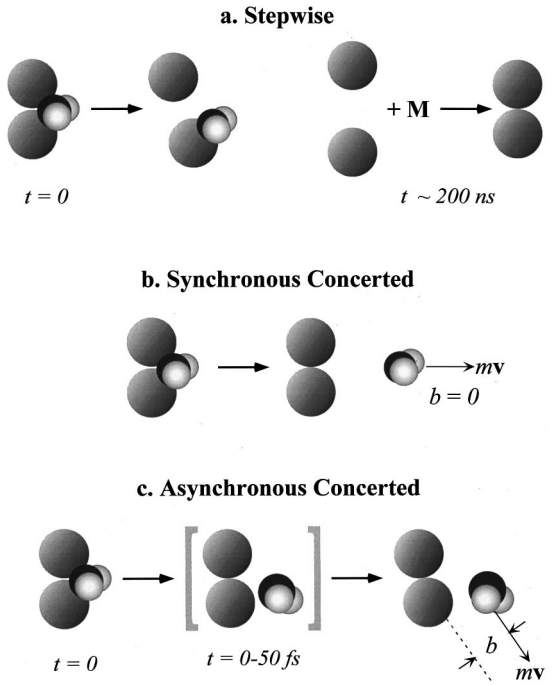

FIG. 7. Possible photoinduced molecular detachment mechanisms for CH_2I_2. Three mechanisms are depicted. In the stepwise mechanism, one of the two C—I bonds breaks to produce an iodine atom. The iodine atoms form an I_2 molecule following a three body collision. This is a nonconcerted mechanism. Under the experimental conditions in this study, three body collisions are extremely rare. The synchronous concerted mechanism involves the breaking of the two C—I bonds and formation of an I—I bond with the C_{2v} symmetry preserved. In the asynchronous concerted mechanism, although breaking of the C—I bonds and formation of the I—I bond happen in a single kinetic step, they happen in a manner such that one C—I bond breaks faster than the other. I_2 detachment with this mechanism results in breaking of the C_{2v} symmetry. Notice that the ''impact parameter'' b is finite in this case and that $b=0$ for the synchronous concerted mechanism.

CH_2 will have relatively high translational and vibrational excitation but low rotational excitation.

The fragments, therefore, contain at least 1.8 eV of translational and internal energies. With the assumption of a three-photon excitation and of I_2 in one of its second tier ion-pair state *f*, *g* or *G*, the formation of CH_2 $(\tilde{b})$ can be ruled out because there is not enough energy available (see Table II). If this is the case, we are left with a limited number of choices, i.e., $CH_2(\tilde{X})+I_2(f,g,G)$ and $CH_2(\tilde{a})+I_2(f,g,G)$. Which of these channels is responsible for photodissociation of CH_2I_2 to yield I_2 fluorescence at 272 nm remains to be investigated.

D. Photodissociation mechanism

Figure 7 illustrates several possible I_2 detachment mechanisms for CH_2I_2. In the stepwise mechanism as shown in Fig. 7(a), one of the two C—I bonds breaks to form an iodine atom, which then collides with another iodine atom in a three-body collision to form an I_2 molecule. Since collisions are required to form I_2 molecules by this mechanism, the time to form I_2 is expected to be longer than 100 ns under our experimental conditions. Furthermore, no vibrational coherence would be expected in the nascent I_2 photofragments. Since we have observed vibrational coherence in I_2 and we have found that the time for I_2 formation is extremely fast (<50 fs), this mechanism can clearly be ruled out.

The remaining two mechanisms as shown in Figs. 7(b) and 7(c) are both concerted; namely, breaking of the two C—I bonds and formation of the I—I bond happen in a single kinetic step. The difference between the synchronous concerted mechanism in Fig. 7(b) and the asynchronous concerted mechanism in Fig. 7(c) is that the former preserves the C_{2v} symmetry of the parent molecule CH_2I_2 while the latter does not. In the asynchronous concerted mechanism, one of the C—I bonds breaks earlier, or faster to be more precise, than the other. As we will show in the following discussion, the observed high rotational excitation in the I_2 fragment will furnish sufficient evidence for us to distinguish between these two mechanisms.

Due to the heavy masses of the iodine atoms, the *B* and *C* rotational constants of the CH_2I_2 ground state are very similar to the *B* rotational constant of I_2, with a value of approximately 0.02 cm^{-1}.[16] This gives a rotational distribution in a room temperature sample of CH_2I_2 peaking at $j\sim100$. This is much smaller than the measured center of rotational distribution for the I_2 dissociation products ($j_{max}\approx350$). In fact, there is a difference of about $250\approx$ in angular momentum between the parent CH_2I_2 and the I_2 fragment. If all $250\approx$ were to go into the rotation of the CH_2 fragment, a simple BJ^2 argument predicts that the amount of rotational energy would be on the order of 60 eV! This is clearly impossible; in fact, as we have discussed previously, rotational motion imparted to the CH_2 fragment will be negligible upon I_2 detachment from CH_2I_2. Instead, CH_2 gains a large amount of translational excitation.

As is well known, conservation of angular momentum demands that the angular momentum of the parent $\mathbf{J}_{CH_2I_2}$ be equal to those of the fragments, $\mathbf{J}_{CH_2}$ and $\mathbf{J}_{I_2}$, plus a so-called orbital angular momentum **L**, or

$$\mathbf{J}_{CH_2I_2}=\mathbf{J}_{CH_2}+\mathbf{J}_{I_2}+\mathbf{L}. \tag{24}$$

Here the orbital angular momentum is produced when the two photofragments CH_2 and I_2 fly apart during the photodissociation process. Due to the large masses of the iodine atoms, the magnitude of the orbital angular momentum, *L*, can be well approximated as that of the CH_2 fragment only,

$$L\approx m_{CH_2}v_{CH_2}b, \tag{25}$$

where m_{CH_2} and v_{CH_2} denote, respectively, the mass and velocity of the CH_2 fragment and the ''impact parameter'' *b* represents the shortest distance between the velocity vector $\mathbf{v}_{CH_2}$ and the center of mass of CH_2I_2 [see Fig. 7(c)]. Since $\mathbf{J}_{CH_2}$ is negligible, we find from (24) that $L\approx250\hbar$.

The synchronous concerted mechanism shown in Fig. 7(b) conserves the C_{2v} symmetry of CH_2I_2. According to this mechanism, CH_2 flies away along the symmetry axis, which passes through the center of mass of CH_2I_2. Thus the impact parameter *b* is zero, which indicates that there is no orbital angular momentum in this case. Clearly, it is inconsistent with the above assertion that *L* should be nonzero. On the other hand, the symmetry breaking, asynchronous concerted mechanism shown in Fig. 7(c) does yield a nonzero

orbital angular momentum because in this case $b \neq 0$. In fact, the previously estimated 1.26 eV translational energy in conjunction with the $250\approx$ orbital angular momentum allows us to estimate the impact parameter b to be approximately 2.7 Å. Thus, the experimentally observed high rotational excitation of the I_2 fragments (at least those fluoresce at 272 nm) indicates that the molecular detachment process happens according to the asynchronous concerted mechanism.

From a rudimentary molecular orbital perspective, Cain *et al.*[14] thoroughly examined the minimum energy path for the insertion reaction between carbene CF_2 and Cl_2 to form CF_2Cl_2. Although the study was specifically on the formation or dissociation pathways of ground-state CF_2Cl_2, the lesson learned is quite general and should have great relevance to the current investigation of the molecular detachment mechanism of CH_2I_2. Cain *et al.* found that the least energy pathway for CF_2 and Cl_2 to approach each other is not the least motion pathway. In other words, the least energy pathway is not the pathway that preserves the C_{2v} symmetry. Instead, the CF_2 prefers to attack the Cl_2 from a position that is neither on the (σ_h) plane bisecting the Cl—Cl bond nor on the Cl—Cl bond axis (C_∞); as CF_2 gradually moves into the σ_h plane, the Cl—Cl bond gets weakened but the C—Cl bonds get strengthened. This pathway is essentially the reverse of the asynchronous concerted mechanism described above for the molecular detachment of CH_2I_2. The underlying reason for the preference of this symmetry breaking pathway has been explained by Cain *et al.*[14] in terms of the interaction of frontier orbitals and the ambiphilic nature of the carbene.

Cain *et al.* also found that the barrier height for $CX_2+Y_2 \rightarrow CX_2Y_2$ (where Y denotes a halogen atom) or the reverse process depends on the highest occupied molecular orbital (HOMO)-lowest unoccupied molecular orbital (LUMO) gap of the halogen molecule Y_2.[14] The lower the gap, the lower the barrier. Since the HOMO-LUMO gap decreases from F_2 to I_2, they concluded that the barrier decreases from CX_2F_2 to CX_2I_2. On the other hand, a higher barrier predicts a higher rotational excitation in the fragments. Therefore, although we did not obtain direct information on the rotational distribution of photofragments from the other gem-dihaloalkanes studied in paper I, the study of Cain *et al.* allows us to predict that CH_2Br_2 and CH_2Cl_2, etc., should give higher rotational excitation in their halogen photofragments.

We have also investigated the possibility of several other photodissociation mechanisms. One of them is worthy of particular attention. This mechanism requires one photon to dissociate one of the C—I bonds and a second photon to dissociate the other C—I bond, while the third photon photoassociates[43] the two iodine atoms thus produced. This will be called a three-step mechanism. The difference between this mechanism and the asynchronous concerted mechanism has to be emphasized. In the asynchronous concerted mechanism, absorption of the three photons happens simultaneously and instantaneously. The bond breaking and bond formation events then take place after absorption of the three photons. Since the photodissociation processes happen within the time duration of the pulse, we can not directly distinguish the two possibilities experimentally unless much shorter laser pulses are used. Therefore, we simulated the dynamics according to the two mechanisms using the procedure outlined in Sec. II B in order to distinguish between them.

Figures 8(a) and 8(b) present the simulated results for the two mechanisms. To obtain the simulation shown in Fig. 8(a), we have assumed that the molecular detachment process proceeds according to the following three steps:

$$\begin{cases} CH_2I_2(\tilde{X}) + h\nu(312\ \text{nm}) \rightarrow CH_2I(\tilde{X}) + I(^2P_{3/2}) + 1.8\ \text{eV at } t=0 \\ CH_2I(\tilde{X}) + h\nu(312\ \text{nm}) \rightarrow CH_2(\tilde{X}) + I(^2P_{1/2}) + 0.3\ \text{eV at } t=32\ \text{fs} \\ I(^2P_{3/2}) + I(^2P_{1/2}) + h\nu(312\ \text{nm}) \rightarrow I_2(f) + 0.6\ \text{eV}, \end{cases} \tag{26}$$

where the excess energies are obtained based on the data given by Baughcum *et al.*[4] The first C—I bond is assumed to break with an excess energy of 1.8 eV to produce an I atom in the ground state $^2P_{3/2}$. The second C—I bond is assumed to break at 32 fs later[44] and with an excess energy of 0.3 eV. In this step, the excited I atom ($^2P_{1/2}$) is assumed to be formed. The third step involves the photoassociation[43] of the two iodine atoms to form I_2 in the f excited state. The possibility of two ground I products has not been considered because photoassociation in the third step to produce $I_2(f)$ is not energetically possible with a 312 nm photon.

We have also examined an alternative bond breaking and formation sequence for the three-step mechanism. Here instead of producing ground I in the first step and excited I in the second step as shown in (26), the first and second photons break the two C—I bonds and form excited I and ground I, respectively. The results of this investigation and those obtained with the pathway shown in (26) both predict an I_2 angular momentum that is inconsistent with our experimental observations (*vide infra*). Thus for clarity, only the pathway in (26) will be considered in the following discussions.

The energetics shown in the following equation have been used for the simulation of the asynchronous concerted mechanism in Fig. 8(b),

$$CH_2I_2(\tilde{X}) + 3h\nu(312\ \text{nm}) \rightarrow CH_2(\tilde{X}) + I_2(f) + 2.7\ \text{eV}. \tag{27}$$

Here the excess energy is taken from Table II of this work.

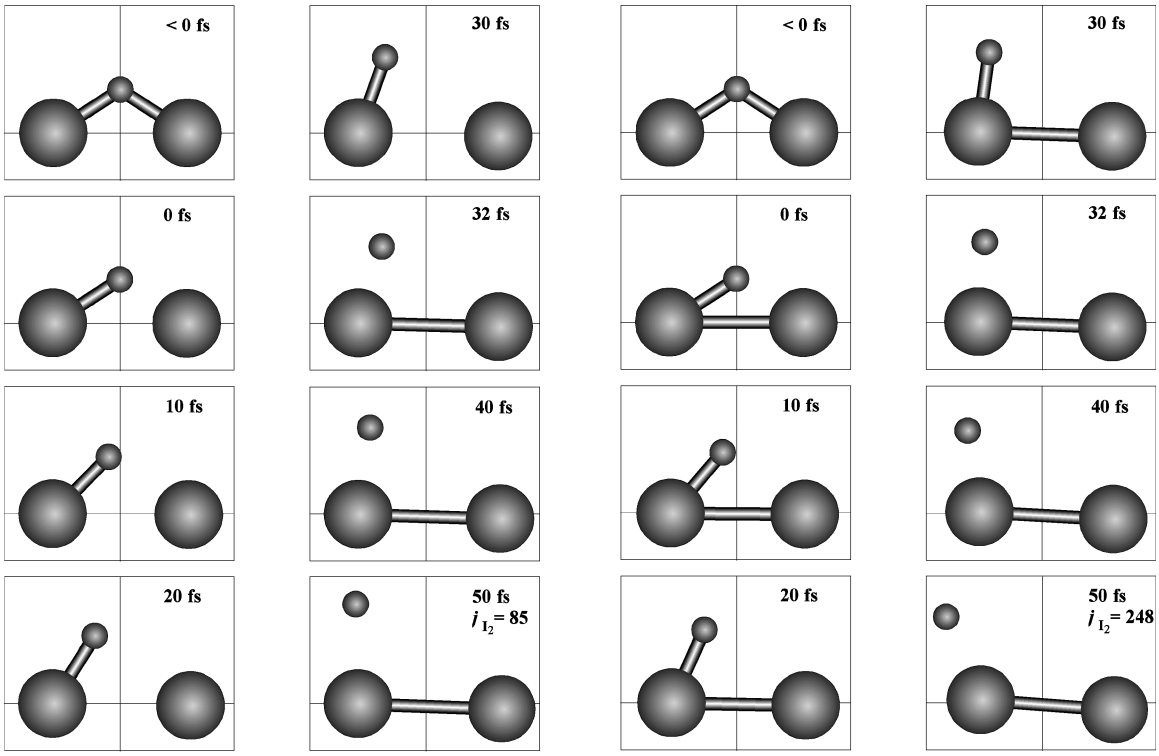

FIG. 8. Classical simulations of molecular detachment processes. In each snapshot, the two large spheres represent the two iodine atoms while the small sphere represents the CH_2 moiety. The simulations were performed for (a) the three-step mechanism and (b) the asynchronous concerted mechanism. The two C—I bond breaking events are assumed to be separated by 32 fs in both mechanisms. In the asynchronous concerted mechanism, the excess energy is estimated to be 2.7 eV for the first bond breakage and zero for the second. The I—I bond is assumed to form immediately after the first bond breaking event. On the other hand, for the three-step mechanism, the excess energy is estimated to be 1.8 eV for the first bond breaking event and 0.3 eV for the second. The I—I bond is assumed to form immediately after the second bond breaking in this case.

The first C—I bond is assumed to break with an excess energy of 2.7 eV. At 32 fs later, the second C—I bond is assumed to break with no excess energy.

Each snapshot in Figs. 8(a) and 8(b) depicts the spatial arrangement of individual atoms (the CH_2 moiety is treated as a pseudoatom) and their bonding configuration at a particular instance. Here, notice that the time reference is chosen to be the instance when the first bond breaks and it may not coincide with the experimental time zero, which is the instance when the pump transition takes place.

Aside from facilitating visualization of the molecular detachment process, a more important purpose of this simulation is to obtain a quantitative estimation of the orbital angular momentum L. This then allows one to compare the estimated L with that obtained from analysis of the experimental data. Since the three (pseudo) atoms in CH_2I_2 are assumed to be motionless before the first bond breaking in this simulation, the triatomic system contains no total angular momentum and will continue not to do so because of conservation of angular momentum. Thus the orbital angular momentum L is the same as the I_2 angular momentum in magnitude but is opposite in sign. The I_2 angular momentum can be calculated readily using the procedure presented in Sec. II B. With a time lag of 32 fs between the two bond breaking events, an I_2 angular momentum of $85\hbar$ is predicted from the three-step mechanism [see Fig. 8(a)] and $248\hbar$ [see Fig. 8(b)] from the asynchronous concerted mechanism. Figure 9 examines how the time lag affects the angular momentum of the I_2 fragment. This figure and Fig. 8 clearly show that the asynchronous concerted mechanism predicts an I_2 angular momentum that is more in agreement with our experimental observations.

E. Identity of the dissociative state of CH_2I_2

Figures 4 and 5 clearly show that there is a high degree of anisotropy as a result of the CH_2I_2 photodissociation process. If each of the transition dipoles corresponding to the three-photon pump transition had different orientations, one would not expect the anisotropy to be so clear. Thus, the three transition dipoles are likely to be parallel to each other. This is further supported by the consideration that the excitation source has femtosecond temporal duration, during which the molecules would not rotate to any significant degree. Therefore, the case where all transition dipoles are parallel becomes the most favorable situation for absorption.

Since CH_2I_2 absorbs one photon at 312 nm and reaches a B_1 state, one expects resonance enhancement if the three-photon process involves the B_1 state as the first transition. If this is the case, the dissociative state reached is expected to be a B_1 electronic state at about 12 eV above the ground state. Although it has been argued that an orbital with B_1 symmetry has a node between the two iodine atoms, this does not necessarily mean that the total wave function (i.e., many electron wave function) with B_1 symmetry should also have no electron density between the two iodine atoms and

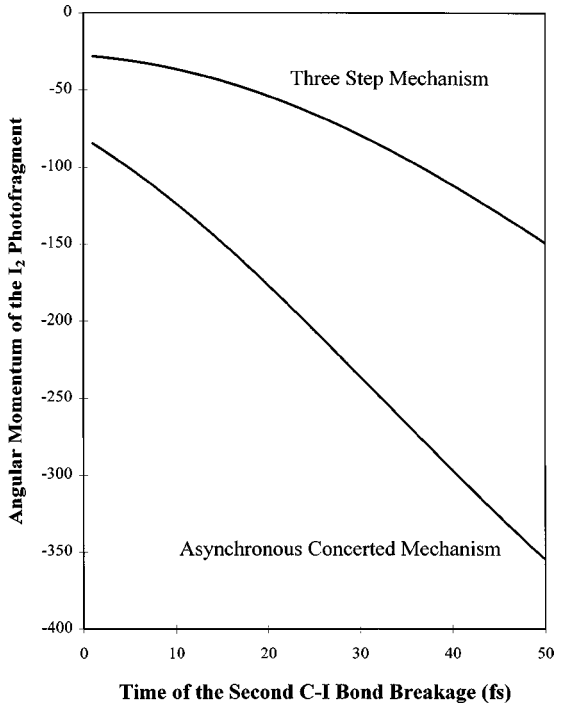

FIG. 9. Dependence of I_2 angular momenta on the time lag between the two bond breaking events. The two traces present the dependencies for the asynchronous concerted mechanism and the three-step mechanism, respectively. The detailed conditions are as stated in Fig. 8.

therefore cannot be responsible for the production of I_2. Since a B_1 transition dipole in this molecule is aligned along the I—I direction (see Fig. 6) and the pump and probe transition dipoles are perpendicular to each other at time zero, the probe transition would be perpendicular to the I_2 bond in this case. However, it is also possible that there is a transition with two-photon resonance enhancement from the ground state, in which case A_1 (parallel to the Z axis) and B_2 (perpendicular to the CH_2 plane) symmetries would be allowed as well.

One might speculate that the multiphoton pump excitation is a charge-transfer transition such that one of the iodine atoms gains electron density while the other loses it during the transition. The electron density redistribution would have the effect of generating a Coulombic attraction between the two iodine atoms while at the same time weakening the two C—I bonds. This is also supported both by the fact that the halogen states that have been observed are all ion-pair, i.e., charge-transfer, states and that molecular dissociation products are not observed until the excitation energy approaches the ionization threshold of the molecule.

V. CONCLUSIONS

In order to extract information about the rotational distribution of photofragments from the experimentally determined rotational anisotropy, we have derived general formulae for rotational anisotropy that are applicable to multiphoton pump and multiphoton probe transitions. We have found that the anisotropy formulation is simple and can be expressed as a constant multiplied by $\langle 1+3\cos\phi_2\rangle_j$ so long as either the pump or the probe is a one-photon transition. If both the pump and probe are multiphoton transitions, the anisotropy can no longer be expressed in such a simple manner. In fact, the conventional definition of the anisotropy loses its meaning of reflecting pure rotational contribution.

Selective detection of fluorescence at 285 and 272 nm from multiphoton excitation of CH_2I_2 reveals a fast ($<$50 fs) I_2 formation and characteristic I_2 vibrational coherence, indicating that the reaction mechanism is concerted. The 272 nm transients also clearly demonstrate fast decaying rotational anisotropy. Least-squares analysis of the anisotropy gives rise to a distribution of rather high I_2 rotational levels, with the distribution center at around $j=350$. This high degree of rotational excitation along with other experimental observations and interpretation allows us to construct the following picture about how we think the photodissociation process of CH_2I_2 happens at an excitation energy of 12 eV.

A three- (312 nm) photon transition excites CH_2I_2 molecules from the thermally populated ground electronic state to a dissociative state; the transition may be of a charge-transfer type. One of the C—I bonds breaks and a bond forms between the two iodine atoms [see the asynchronous concerted mechanism in Fig. 7(c)]; this generates an enormous amount of torque on the CH_2 and I_2 moieties to tear the second C—I bond apart. Dissociation occurs within 50 fs of the initial excitation. The remaining energy from the 12 eV initially deposited in the CH_2I_2 molecule is distributed between the photofragments in the following fashion. During the dissociation, the CH_2 fragment gains a tremendous amount of translational energy and a sizable degree of vibrational excitation but little rotational or electronic excitation. On the other hand, the I_2 fragment is left in a highly excited electronic state with a large amount of rotational excitation but only moderate vibrational excitation and very little translational energy.

Although the 272 nm fluorescence resulting from excitation of CH_2I_2 can in principle be attributed to emission from several ion-pair states of I_2, analysis of the vibrational coherence at this wavelength suggests that one of the I_2 f, g, G states is likely responsible for this fluorescence. The electronic state of the CH_2 fragment has been determined to some extent for this particular dissociation channel by energetic considerations. Assuming three-photon excitation of CH_2I_2, and taking into consideration the high translational energy imparted into the CH_2 fragment and the relatively high rotational energy in the I_2 fragment, we have argued that the CH_2 fragment is quite possibly in its ground ($\tilde{X}$) or first excited ($\tilde{a}$) electronic state. Time-of-flight mass spectrometry following photodissociation of CH_2I_2 in the molecular beam will allow us to analyze the final electronic state of the CH_2 fragments.

ACKNOWLEDGMENTS

We would like to thank Dr. S. Baskin and Professors J. C. Polanyi, S. Stolte, A. Stolow, P. Corkum, and M. Ivanov for helpful discussions. This work was partially supported by a Camille and Henry Dreyfus New Faculty Award. M.D. is a Beckman Young Investigator and a Packard Science and Engineering Fellow.

[1] U. Marvet, Q. Zhang, E. J. Brown, and M. Dantus, J. Chem. Phys. **109**, 4415 (1998), preceding paper.
[2] M. Kawasaki, S. J. Lee, and R. Bersohn, J. Chem. Phys. **63**, 809 (1975).
[3] P. M. Kroger, P. C. Demou, and S. J. Riley, J. Chem. Phys. **65**, 1823 (1976).
[4] S. L. Baughcum and S. R. Leone, J. Chem. Phys. **72**, 6531 (1980).
[5] W. H. Pence, S. L. Baughcum, and S. R. Leone, J. Phys. Chem. **85**, 3844 (1981).
[6] T. F. Hunter and K. S. Kristjansson, Chem. Phys. Lett. **90**, 35 (1982).
[7] J. Zhang and D. G. Imre, J. Chem. Phys. **89**, 309 (1988).
[8] J. Zhang, E. J. Heller, D. Huber, D. G. Imre, and D. Tannor, J. Chem. Phys. **89**, 3602 (1988).
[9] B. J. Schwartz, J. C. King, J. Z. Zhang, and C. B. Harris, Chem. Phys. Lett. **203**, 503 (1993).
[10] W. M. Kwok and D. L. Phillips, Chem. Phys. Lett. **235**, 260 (1995).
[11] W. M. Kwok and D. L. Phillips, J. Chem. Phys. **104**, 2529 (1996).
[12] K. Saitow, Y. Naitoh, K. Tominaga, and K. Yoshihara, Chem. Phys. Lett. **262**, 621 (1996).
[13] F. Duschek, M. Schmitt, P. Vogt, A. Materny, and W. Kiefer, J. Raman Spectrosc. **28**, 445 (1997).
[14] S. R. Cain, R. Hoffmann, and E. R. Grant, J. Phys. Chem. **85**, 4046 (1981).
[15] M. N. Glukhovtsev and R. D. Bach, Chem. Phys. Lett. **269**, 145 (1997).
[16] Z. Kisiel, L. Pszczolkowski, W. Caminati, and P. G. Favero, J. Chem. Phys. **105**, 1778 (1996).
[17] U. Marvet and M. Dantus, Chem. Phys. Lett. **256**, 57 (1996).
[18] U. Marvet, Q. Zhang, and M. Dantus, J. Phys. Chem. A **102**, 4111 (1998).
[19] Q. Zhang, U. Marvet, and M. Dantus, Faraday Discuss. **108**, 63 (1997).
[20] C. Fotakis, M. Martin, and R. J. Donovan, J. Chem. Soc., Faraday Trans. 2 **78**, 1363 (1982).
[21] H. Okabe, M. Kawasaki, and Y. Tanaka, J. Chem. Phys. **73**, 6162 (1980).
[22] P. J. Dyne and D. W. G. Style, J. Chem. Soc. **1952**, 2122.
[23] D. W. G. Style and P. J. Dyne, J. Chem. Soc. **1952**, 2125.
[24] G. Black, *Research on High Energy Storage for Laser Amplifiers* (Stanford Research Institute, 1976).
[25] I. Pastirk, E. J. Brown, Q. Zhang, and M. Dantus, J. Chem. Phys. **108**, 4375 (1998).
[26] R. G. Gordon, J. Chem. Phys. **45**, 1643 (1966).
[27] A. B. Myers and R. M. Hochstrasser, J. Chem. Phys. **85**, 6301 (1986).
[28] P. M. Felker, J. S. Baskin, and A. H. Zewail, J. Phys. Chem. **90**, 724 (1986).
[29] P. M. Felker and A. H. Zewail, J. Chem. Phys. **86**, 2460 (1987).
[30] A. H. Zewail, J. Chem. Soc., Faraday Trans. 2 **85**, 1221 (1989).
[31] M. Dantus, R. M. Bowman, J. S. Baskin, and A. H. Zewail, Chem. Phys. Lett. **159**, 406 (1989).
[32] J. S. Baskin and A. H. Zewail, J. Phys. Chem. **98**, 3337 (1994).
[33] G. Arfken, *Mathematical Methods for Physicists*, 3rd ed. (Academic, New York, 1985).
[34] MATHEMATICA (3.0), Wolfram Research, Inc. (Wolfram Media, Champaign, IL, 1996).
[35] L. D. Landau and E. M. Lifshitz, *Mechanics*, 3rd ed. (Pergamon, Oxford, 1976).
[36] G. Herzberg, *Molecular Spectra and Molecular Structure* (Van Nostrand Reinhold, New York, 1945).
[37] *CRC Handbook of Chemistry and Physics*, edited by R. C. Weast and M. J. Astle (CRC, Boca Raton, Florida, 1982), Vol. 63.
[38] K. Lawley, P. Jewsbury, T. Ridley, P. Langridge-Smith, and R. Donovan, Mol. Phys. **75**, 811 (1992).
[39] P. J. Wilson, T. Ridley, K. P. Lawley, and R. J. Donovan, Chem. Phys. **182**, 325 (1994).
[40] K. S. Viswanathan, A. Sur, and J. Tellinghuisen, J. Mol. Spectrosc. **86**, 393 (1981).
[41] K. S. Viswanathan and J. Tellinghuisen, J. Mol. Spectrosc. **101**, 285 (1983).
[42] G. Herzberg, *Molecular Spectra and Molecular Structure* (Krieger, Malabar, Florida, 1991).
[43] See, for example, U. Marvet and M. Dantus, Chem. Phys. Lett. **245**, 393 (1995) and P. Gross and M. Dantus, J. Chem. Phys. **106**, 8013 (1997), and references therein.
[44] When the two C–I bond breaking events are separated by 32 fs, simulation of the asynchronous concerted mechanism predicts an angular momentum quantum number of 248 for I_2.